A Destruction-Free Parameter Extraction Scheme for GTO Models

L. Göhler, T. Langer*, J. Sigg*

Universität der Bundeswehr München, Werner-Heisenberg-Weg 39, D-85577 Neubiberg, Germany
Tel.: +49-89-6004-3665, Fax: +49-89-6004-2223, email: Lutz.Goehler@unibw-muenchen.de
*Siemens AG, Corporate Technology, Munich, Germany

Abstract–This paper presents a physically based parameter extraction scheme for GTO models. The methods are discussed and demonstrated with an example. The comparison between simulated and measured device behaviour shows good agreement.

I. Introduction

In recent years research has been concentrated on the development of power device models, but very often parameter determination was not considered sufficiently. These values were assumed to be given, although even the manufacturer can not provide all required information. Therefore the focus of this paper is directed towards this deficit.

Pure curve-fitting (automated or by trial and error) of a given model to measured transients and DC-characteristics may lead to satisfying results, but there is still an uncertainity, whether the initial values of that optimization are precise enough to obtain a parameter set, which allows the model to reproduce the whole range of operation.

For comparatively simple models with only a few not very complex equations one can use derivations of these model equations for extraction [1]. Normally there is no further refinement of the parameter set necessary. In contrast, most more accurate models consist of a large number of equations (explicit and implicit) or are completely numerical. In this case it is of utmost importance to derive appropriate measurement methods for parameter determination.

All extraction methods described in the following are non-destructive and require electrical measurements only.

II. Parameter Extraction Scheme

A. Parameter Set

The parameter set, consisting of 16 parameters, corresponds to the model of an anode-shorted GTO in [2] (see Fig. 1 and Table I).

TABLE I
Parameter Set

Parameter	Physical Meaning
A	Active area
N_{b1}	Doping of the n-base
N_{b2}	Peak doping of the p-base
N_{e1}	Peak doping of the p-emitter
N_{e2}	Peak doping of the n-emitter
w_{b1}	Width of the n-base
w_{b2}	Width of the p-base
w_{e1}	Width of the p-emitter
w_{e2}	Width of the n-emitter
τ_{b1}	Minority carrier lifetime (n-base)
τ_{b2}	Minority carrier lifetime (p-base)
I_{se1}	Saturation current (elec. inj., p-emitter)
I_{se2}	Saturation current (hole inj., n-emitter)
R_s	Short resistance
V_{brga}	Breakdown voltage ($n^- - p$-junction)
V_{brgc}	Breakdown voltage ($p - n^+$-junction)

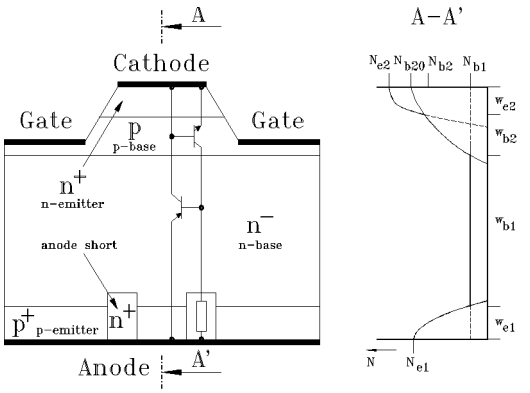

Fig. 1. Structure of an anode-shorted GTO with equivalent circut and doping profile.

Additional values, such as thermal resistances and capacitances, are taken from the data book.

B. Extraction of the Doping Parameters

By measuring the capacitance C_j of the reverse biased middle junction the uniform n-base doping and the doping profile parameters of the p-base can be extracted (Fig. 2). Since the positive anode-gate bias voltage V_r

forces the shorted p-emitter-n-base-junction in forward mode its capacity has a considerably larger value than C_j. Consequently, the resulting capacitance equals C_j in good approximation.

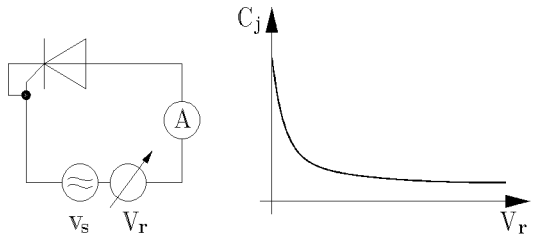

Fig. 2. Junction capacitance measurement.

Measured C_j (V_r) data are transferred to a device simulator with a built-in optimizer, such as MEDICI, to get the doping parameters N_{b1}, N_{b20} (p-doping at peak emitter doping), A and the sum of p-base and n-emitter width $w_{b2}+w_{e2}$. As the GTO model presupposes a Gaussian p-base doping profile this profile type should be selected in the device simulator, too. The less dimensions optimization has the easier a solution is found. Assuming that N_{b1} dominates C_j at the maximum V_r gives the opportunity to save one dimension:

$$A \approx C_{j\,min}\sqrt{\frac{2V_{r\,max}}{q\varepsilon_0\varepsilon_r N_{b1}}}. \tag{1}$$

The capacitance of the reverse biased p-base-n-emitter-junction found from an equivalent experiment enables to determine N_{b20}, N_{e2} and w_{e2}, which vice versa delivers w_{b2}. Due to the shorts N_{e1} and w_{e1} can be estimated only.

As an alternative to device simualtions the approximation

$$\exp\left(-\frac{x^2}{\lambda^2}\right) \approx \frac{a_1}{1+\exp\left(\frac{a_2}{\lambda}x+a_3\right)} \tag{2}$$

allows to calculate the capacitance of a diffused layer junction (a_1, a_2, a_3=const.). Based on that, a suitable optimizer, such as CYNOSURE, performes the least-square fit.

C. Determination of the Breakdown Voltages

The middle junction is reverse biased again (Fig. 3). V_{brga} equals that voltage the anode current starts to increase rapidly for.

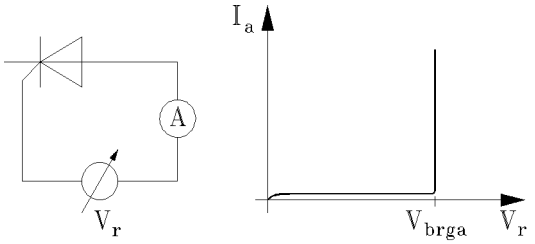

Fig. 3. Breakdown voltage measurement.

An analogous measurement setup for the p-base-n-emitter- junction provides V_{brgc}.

D. Determination of the n*-Base Lifetime*

In forward conduction mode electrons and holes are stored in the n- and p-base (Fig. 4, $Q_{b1} \gg Q_{b2}$). During the tail phase at constant voltage V_{ac} (Fig. 5, 6) excess carriers mainly vanish by recombination until the device blocks. Therefore the charge control equation takes the following form:

$$\frac{Q_{b1}}{\tau^*_{an}} + \frac{\mathrm{d}Q_{b1}}{\mathrm{d}t} \approx 0 \tag{3}$$

or

$$\frac{I_A}{\tau^*_{an}} + \frac{\mathrm{d}I_A}{\mathrm{d}t} \approx 0, \tag{4}$$

when the carrier distribution in the n-base has a linear shape. The variable I_A denotes the anode current and τ^*_{an} stands for the current-dependent high-level injection lifetime. Solving (4) for I_A leads to

$$I_A(t) = I_{TAIL}\exp\left(-\frac{t-t_0}{\tau^*_{an}}\right), \tag{5}$$

so that τ^*_{an} follows from $\frac{dI_A}{dt}\big|_{t=t_0}$ easily.

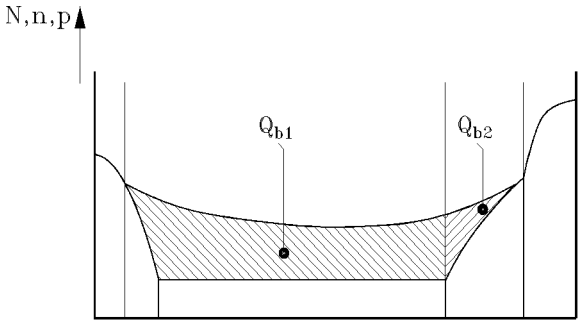

Fig. 4. Charge in the n-base and the p-base under static conditions ($Q_{b1} \gg Q_{b2}$).

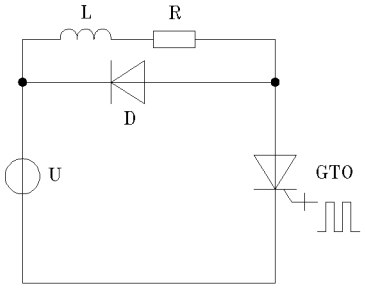

Fig. 5. Measuring circuit for n-base carrier lifetime (U = 400V, L = 3.7mH, R = 1.1Ω, D : SSiN 46, GTO : G90)

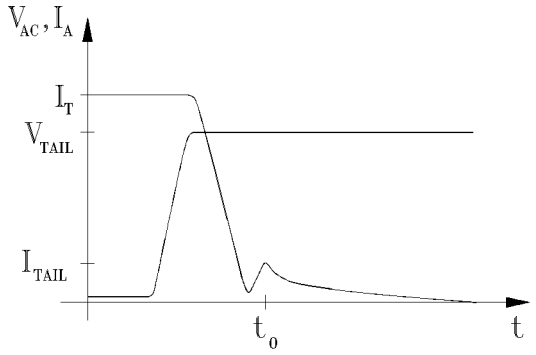

Fig. 6. Current waveform for switch-off without snubber circuit.

Due to emitter backinjection τ_{an}^* depends on the anode current I_T. Hence, τ_{b1} equals the limit of τ_{an}^* for $I_f \to 0$:

$$\tau_{b1} \approx \frac{1}{2} \lim_{I_f \to 0} \tau_{an}^*. \tag{6}$$

The factor 0.5 derives from Shockley-Read-Hall recombination formula for equal minority carrier liftime in n- and p-type silicon.

Another method, also based on tail current evaluation, presents [4].

E. Determination of the n*-Base Width*

According to [4] one can assume a negligible small loss of charge in the n-base between the application of a negtive gate signal and the onset of tail current. If, furthermore, the anode-cathode voltage V_{ac} remains constant over that time span, the n-base carrier distribution changes to a linear one. From a comparison of the static currents and charges (e.g. before switch-off) with the situation in the tail phase the following equation results for the n-base width:

$$0 = \frac{I_T}{I_{TAIL}} - \frac{1}{2}\left(\frac{w_{b1}}{L_{b1}}\right)^2 \frac{\cosh\left(\frac{w_{b1}}{L_{b1}}\right)}{\cosh\left(\frac{w_{b1}}{L_{b1}}\right) - 1}, \tag{7}$$

where L_{b1} stands for the ambipolar diffusion length in the n-base and I_{TAIL} denotes the maximum tail current. Further simplification yields:

$$w_{b1} \approx L_{b1}\sqrt{2\frac{I_T}{I_{TAIL}}}. \tag{8}$$

To keep V_{ac} constant a large snubber capacitance is required (Fig. 7, 8). The anode current I_T should be chosen as small as possible to reduce backinjection of electrons into the p-emitter.

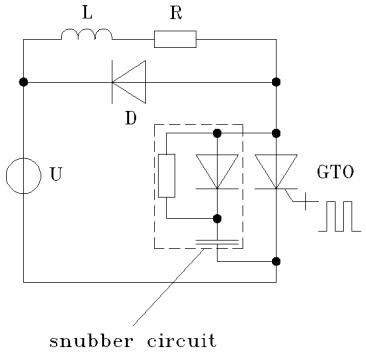

Fig. 7. Measuring circuit for n-base carrier lifetime (U = 400V, L = 3.7mH, R = 1.1Ω, D : SSiN 46, GTO : G90, Snubber: R = 3.6Ω, C = 12.2μF, D : SSiN 46)

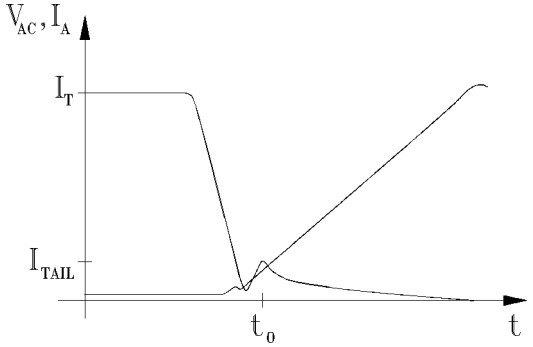

Fig. 8. Current waveform for switch-off with large snubber capacitance.

In some cases w_{b1} corresponds to the measured breakdown voltage V_{brga}. If V_{brga} is smaller than the value expected from n-base doping [3], the current increases due to punch trough:

$$w_{b1} = \sqrt{\frac{2\varepsilon_0\varepsilon_r V_{brga}}{qN_{b1}}}. \tag{9}$$

F. Determination of the p*-Base Lifetime*

Normally the high-level injection lifetime in the n-base ($2 \cdot \tau_{b1}$) equals that in the p-base near the middle junction, but doping dependence of lifetime should not be neglected. Using the results by Roulston [5] and Scharfetter, $\tau_{b2}(x)$ becomes (Fig. 9):

$$\tau_{b2}(x) = \frac{\tau_{b20}}{1 + \frac{N(x)}{N_{ref}}} \tag{10}$$

with $\tau_{b20} \approx \tau_{b1}$ and $N_{ref} \approx 3{\cdot}10^{15}\mathrm{cm}^{-3}$. The identity of τ_{b1} and the maximum minority carrier lifetime τ_{b20} explains again from the assumption of equal lifetime in n- and p-type silicon.

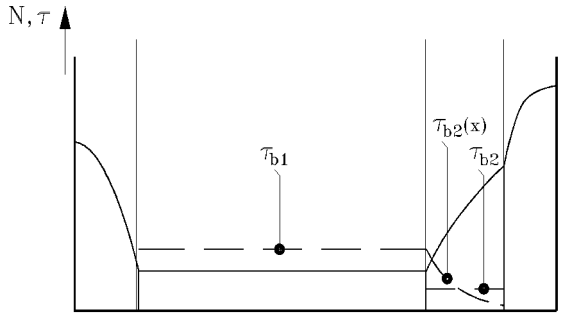

Fig. 9. Minority carrier lifetime in the n-base and the p-base.

A common approach for the effective p-base lifetime evaluates the integral of $1/\tau_{b2}(x)$ over w_{b2}:

$$\frac{1}{\tau_{b2}} = \frac{1}{w_{b2}} \int_{w_{e2}}^{w_{e2}+w_{b2}} \frac{\mathrm{d}x}{\tau_{b2}(x)}, \tag{11}$$

expressing, that the recombination term in the ambipolar diffusion equation does not change when using the effective lifetime instead of the doping dependent one. Inserting (2) into (11) leads to:

$$\begin{aligned} \frac{1}{\tau_{b2}} &= \frac{1 + \frac{N_{b1}}{N_{ref}}}{\tau_{b1}} + \frac{a_1 \lambda N_{b20}}{a_2 w_{b2} \tau_{b1} N_{ref}} \ln(f_1), \qquad (12) \\ f_1 &= \frac{1 + \exp\left(-\frac{a_2}{\lambda} w_{e2} - a_3\right)}{1 + \exp\left(-\frac{a_2}{\lambda}(w_{e2} + w_{b2}) - a_3\right)}. \end{aligned}$$

G. Determination of the Saturation Currents

With known emitter doping profiles device simulations of the interesting p-n-junctions are an elegant way to obtain the saturation currents.

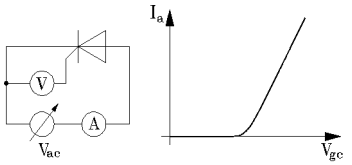

Fig. 10. Measuring the anode current as a function of gate-cathode voltage.

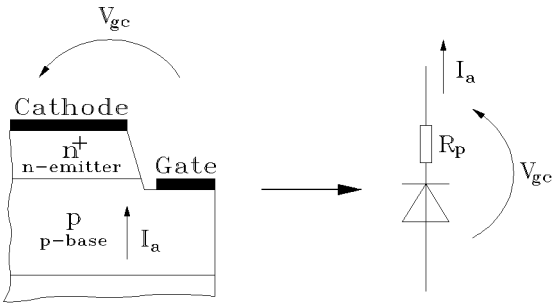

Fig. 11. GTO structure and equivalent circuit for $I_a = f(V_{gc})$ measurement.

Alternatively, the anode current of the ignited GTO is plotted versus the gate-cathode voltage (Fig. 10, 11). The saturation currents of backinjection are obtained by fitting this curve to the model equations in static case for both the p^+n^- and the $n^+ - p$-junction. This method facilitates to ignore the base resistance and forces the current to flow along the main current path. Measuring the characteristic dynamically limits self-heating of the device. Fig. 11 shows the GTO's cathode region and the corresponding circuit.

The v-i-characteristic of the n-emitter-p-base-junction has the following form (D_n diffusion constant for electrons, L_{b2} ambipolar diffusion length in the p-base):

$$\begin{aligned} I_a &= \frac{2qAD_n n_i^2}{N_{b2} L_{b2} \tanh\left(\frac{w_{b2}}{L_{b2}}\right)} \times \\ &\quad \left(\exp\left(\frac{V_{gc}^*}{mV_T}\right) - 1\right) + \left(1 + \frac{\mu_n}{\mu_p}\right) I_{se2} \frac{n_i^2}{N_{b2}^2} \times \\ &\quad \left(\exp\left(\frac{2V_{gc}^*}{mV_T}\right) - 1\right), \qquad (13) \end{aligned}$$

which can be transformed to take into account the parasitic resistance R_p (V_T: thermal voltage):

$$\begin{aligned} V_{gc} &= mV_T \ln(f_0) + I_a R_p, \qquad (14) \\ f_0 &= \frac{f_1}{2f_2}\left(\sqrt{1 + \frac{4f_2^2}{f_1^2}\left(\frac{f_1}{f_2} + \frac{I_a}{f_2} + 1\right)} - 1\right), \\ f_1 &= \frac{2qAD_n n_i^2}{N_{b2} L_{b2} \tanh\left(\frac{w_{b2}}{L_{b2}}\right)}, \end{aligned}$$

$$f_2 = \left(1+\frac{\mu_n}{\mu_p}\right) I_{se2} \frac{n_i^2}{N_{b2}^2}.$$

This leads to I_{se2}, R_p and m. The function of m is to incorporate the remaining self-heating. With the eliminated voltage drop due to R_p a least-square fit of that curve to the anode current as a function of V_{am} (effective voltage across p-emitter-n-base-junction) yields I_{se1}:

$$I_a = \frac{2qAD_p n_i^2}{N_{b1}L_{b1}\tanh\left(\frac{w_{b1}}{L_{b1}}\right)}\left(\exp\left(\frac{V_{am}}{mV_T}\right)-1\right) + \left(1+\frac{\mu_p}{\mu_n}\right) I_{se1}\frac{n_i^2}{N_{b1}^2} \times \left(\exp\left(\frac{2V_{am}}{mV_T}\right)-1\right). \quad (15)$$

The difference between V_{gc}^* and V_{am} may be seen as constant:

$$V_{am} \approx V_{gc}^* - V_d \quad (16)$$

H. Determination of the Short Resistance

R_s is adjusted so that the minimum gate trigger current of the model equals the value given in the manufacturer's data sheet.

III. Results

All extraction routines were performed for a small GTO ($I_{TQRM} = 90A$) to prove the concept. In Table II a comparison is displayed between data given by the manufacturer or obtained from fitting the model to best agreement with measurement and extracted parameters. In transient simulation (Fig. 14, 15) one can observe larger oscillations when using the extracted parameters, but the gate charge differs for 10% only. The difference in the DC-currents (Fig. 12, 13) is large, but mainly caused by the failure of the very sensitive parameter w_{b2}. Changing this value to the correct one produces a nearly perfect agreement. It is clearly to be seen, that the extracted parameters meet manufacturer data.

IV. Conclusion

A physically based parameter extraction scheme for GTO models is presented. The comparison with manufacturer data proves a good agreement. Some of the procedures, such as junction capacity measurement, minority carrier lifetime determination and the extraction of the n-base width can be applied to other power devices, too. All methods are destruction-free.

TABLE II
Comparison between Manufacturer/Fitted Data and Extracted Parameters

Parameter	Manufacturer/Fit	Extracted
$A[\mathrm{cm}^2]$	0.64	0.69
$N_{b1}[\mathrm{cm}^{-3}]$	$3\cdot10^{13}$	$4.9\cdot10^{13}$
$N_{b2}[\mathrm{cm}^{-3}]$	$4\cdot10^{16}$	$5.3\cdot10^{16}$
$N_{e1}[\mathrm{cm}^{-3}]$	$2\cdot10^{19}$	$1\cdot10^{19}$
$N_{e2}[\mathrm{cm}^{-3}]$	$1\cdot10^{20}$	$4.4\cdot10^{20}$
$w_{b1}[\mu\mathrm{m}]$	230	244
$w_{b2}[\mu\mathrm{m}]$	40	20
$w_{e1}[\mu\mathrm{m}]$	64	43
$w_{e2}[\mu\mathrm{m}]$	17	23
$\tau_{b1}[\mu\mathrm{s}]$	2	1.7
$\tau_{b2}[\mu\mathrm{s}]$	0.49	0.34
$I_{se1}[\mathrm{A}]$	$4\cdot10^{-11}$	$1.1\cdot10^{-12}$
$I_{se2}[\mathrm{A}]$	$2\cdot10^{-14}$	$7.1\cdot10^{-14}$
$R_s[\Omega]$	0.4	0.4
$V_{brga}[\mathrm{V}]$	1440	1440
$V_{brgc}[\mathrm{V}]$	18.8	18.8

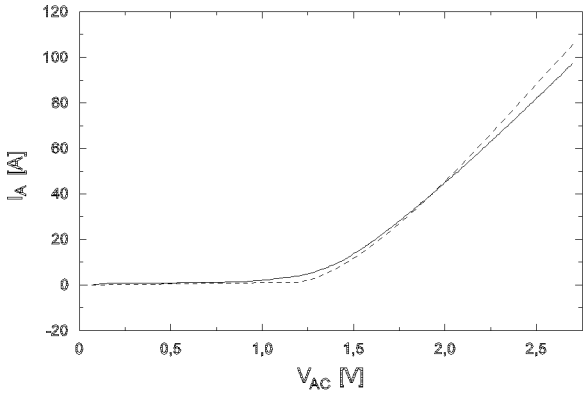

Fig. 12. Comparison between measurement (—) and simulation (- -) of DC-characteristic with manufacturer/fitted data.

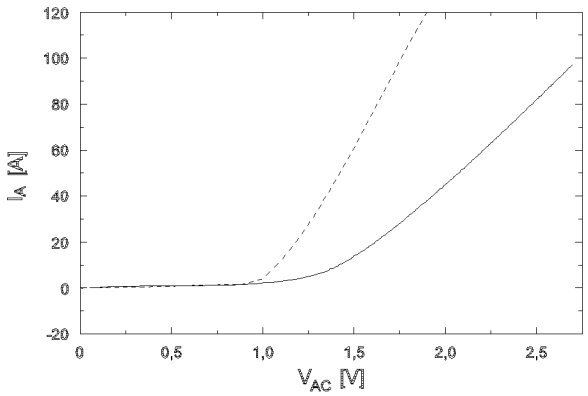

Fig. 13. Comparison between measurement (—) and simulation (- -) of DC-characteristic with extracted parameters.

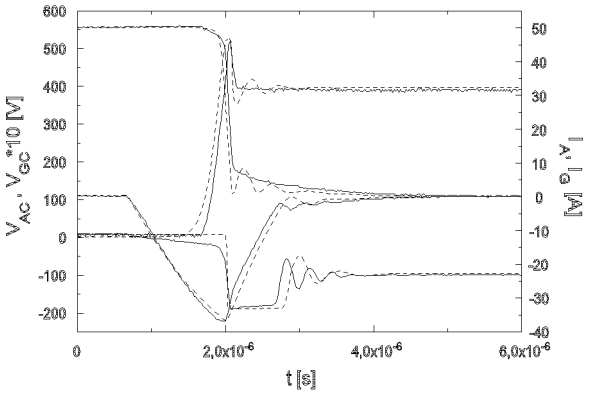

Fig. 14. Comparison between measurement (—) and simulation (- -) of switch-off with manufacturer/fitted data.

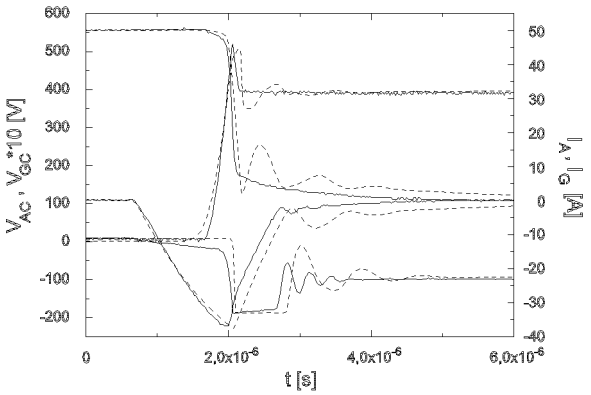

Fig. 15. Comparison between measurement (—) and simulation (- -) of switch-off with extracted parameters.

References

[1] H. Güldner, K. Lehnert, B. Arlt, L. Göhler, Adaptation of a Power Diode Model to PSPICE, Proc. of PCIM '95.

[2] M. Bayer, R. Kraus, K. Hoffmann, A New Analytical GTO Model for Circuit Applications, Proc. of PESC '95.

[3] S. K. Ghandi, Semiconductor Power Devices, John Wiley & Sons, Inc., 1977.

[4] D. Metzner, Netzwerkmodelle abschaltbarer Leistungshalbleiter-Bauelemente, Thesis, TU München, 1994.

[5] D. J. Roulston, N. D. Arora, S. G. Chamberlain, Modeling and Measurement of Minority-Carrier Lifetime versus Doping in Diffused Layers of $n^+ - p$ Silicon Diodes, IEEE Trans. on Electron Devices, vol. 29, No. 2, February 1982.